



Cite this: DOI: 10.1039/d4sm01497a

## Absorbing-state transitions in particulate systems under spatially varying driving

Bhanu Prasad Bhowmik \* and Christopher Ness

Non-equilibrium transitions into absorbing states are widespread, and amorphous materials under cyclic shear have emerged as useful model systems in which to study their properties. Recent work has focused on homogeneous driving in which the shear amplitude is uniform in space, despite most real world flows involving spatially inhomogeneous conditions that are known to produce qualitatively distinct phenomenology. Here we study the absorbing state transition under inhomogeneous driving using a modified random organization model. For smoothly varying driving the steady state results map onto the homogeneous absorbing state phase diagram, with the position of the boundary between absorbing and diffusive states being insensitive to the driving wavelength. The phenomenology is well-described by a one-dimensional generalized continuum model that we pose. For discontinuously varying driving the position of the absorbing phase boundary and the exponent characterising the fraction of active particles are altered relative to the homogeneous case.

 Received 17th December 2024,  
 Accepted 21st March 2025

DOI: 10.1039/d4sm01497a

[rsc.li/soft-matter-journal](https://rsc.li/soft-matter-journal)

### 1. Introduction

Soft materials under cyclic deformation exhibit rich phenomenology including self-organized criticality,<sup>1</sup> mechanical annealing,<sup>2</sup> yielding,<sup>3</sup> fatigue failure,<sup>4</sup> and absorbing state transitions.<sup>5</sup> The latter separate states where on one side the system remains stuck indefinitely due to the absence of dynamics, and on the other is ever-diffusing. They are relevant to applications such as liquefaction<sup>6</sup> and hopper unblocking,<sup>7</sup> while recent fundamental work has advanced basic understanding of non-equilibrium physics,<sup>5,8–13</sup> with implications for broader areas such as infectious disease, reaction-diffusion dynamics, and forest fire propagation.<sup>1</sup>

In athermal particulate systems under cyclic deformation with driving amplitude  $\gamma$  less than a volume (or area) fraction  $\phi$  dependent threshold  $\gamma_c(\phi)$ , such systems attain special configurations which reappear precisely after full cycles of deformation so that, when viewed stroboscopically (with a period of 1 or occasionally more cycles<sup>14</sup>), the system does not explore configuration space. Above  $\gamma_c$  there exist active particles ( $C_A$ ) that do not return to their initial positions so that the self-diffusion coefficient is nonzero. These states are separated by a critical line on the  $\phi$ - $\gamma$  phase diagram, exhibiting an equilibrium-like continuous transition with  $C_A$  serving as the order parameter. To study the physics of this transition it has proven useful to explore ‘random organization’ models,<sup>5,15–18</sup> whose predictions suggest that it belongs to the conserved directed percolation (CDP) class, though this is altered in the presence of multiple or mediated interactions.<sup>19,20</sup>

Thus far, such models are reported for homogeneous driving only, yet in practical scenarios involving cyclic driving of particulates the driving rate may inherently be non-uniform. More broadly, the role of spatial inhomogeneity in processes with absorbing states is relevant to regionally varying immunity levels in disease spreading scenarios, or to reaction-diffusion problems with spatially varying catalytic activity. Moreover recent studies on various soft materials<sup>21–26</sup> reveal that the rheology of systems under homogeneous and inhomogeneous driving often differs qualitatively, so that the response to the latter cannot necessarily be fully predicted based on the former. Thus, in order to gain fundamental insight into this more complex class of problems it is crucial to determine whether the presence of spatially varying driving forces affects the nature and position of absorbing state transitions in discrete systems, and, importantly, whether homogeneous measurements predict the properties of inhomogeneous systems.

We use a modified isotropic random organization model<sup>15,27</sup> to study the absorbing state transition under inhomogeneous driving. The control parameters are the overall area fraction  $\bar{\phi}$  of particles of diameter  $\sigma$  and their per-step displacement  $\Delta$ . The latter is an analogue of the oscillatory strain amplitude  $\gamma$ , and we impose spatial dependence  $\Delta(y)$  to represent, *e.g.*, the spatially varying strain rate present in a flowing system. For diffusive states we observe in the results a spatial inhomogeneity with the local area fraction at  $y$ ,  $\phi(y)$ , being lower in regions where the driving amplitude  $\Delta(y)$  is large. For smoothly varying driving ( $\partial\Delta/\partial y$  exists at every point) with  $L_y/\sigma = 7.7$ –400, the local active particle concentration  $C_A(y)$  matches that obtained under homogeneous conditions at the same  $\Delta(y)$  and  $\phi(y)$ , indicating that the presence of gradients does not influence the properties of

School of Engineering, University of Edinburgh, Edinburgh EH9 3JL, UK.  
 E-mail: [bhowmikbhanuprasad592@gmail.com](mailto:bhowmikbhanuprasad592@gmail.com)

the  $\Delta$ - $\phi$  phase diagram. Here,  $L_y/\sigma$  is the length of periodicity in  $\Delta(y)$ . We thus explore a continuum model modified to account for inhomogeneous driving, and find that it supports the results of our simulation, which predicts the expected mean-field exponents.<sup>28,29</sup> Conversely, for discontinuous  $\Delta(y)$  inhomogeneous effects play a role and the properties of the phase diagram depend on the length  $L_c$  over which the driving remains uniform. For  $L_c/\sigma \lesssim 20$ , the position of the absorbing boundary depends on  $L_c$ , while for a different case in which  $\Delta = 0$  for a small fraction of particles  $C_p$ , the position and exponent of the transition are  $C_p$ -dependent, indicating a change to the universality class.

## 2. Simulation details

We simulate  $N = 5000$ – $30\,000$  disks with diameter chosen from a Gaussian distribution with mean  $\sigma$  and standard deviation  $0.2\sigma$  in a box of area  $L_x \times L$  (with  $L$  an integer multiple of  $L_y$ , wavelength of the spatial variation in the drive). Initially random configurations having widespread particle overlaps evolve according to the following deterministic rules. Particles not overlapping with any other are inactive and do not move. Particles with  $Z > 0$  overlapping neighbours are active and their positions  $\mathbf{r}_i$  are updated following  $\mathbf{r}_i(t + \delta t) = \mathbf{r}_i(t) + \Delta_i \delta t \sum_{j=1}^Z \mathbf{n}_{ji}$ ,

where  $\mathbf{n}_{ji}$  are unit vectors pointing to particle  $i$  from each of its contacts  $j$ ,  $\Delta_i$  is the kick size for the  $i$ th particle, and  $\delta t = 1$ . In the absence of any spatial heterogeneity,  $\Delta_i$  is the same for all particles. A comparison between the random organization model and the modified random organization model studied here is

presented in Fig. 1. The overall area fraction is  $\bar{\phi} = \frac{\sum_{i=0}^N \pi \sigma_i^2}{4L_x L}$ . We

produced the  $\Delta$ - $\phi$  phase diagram for spatially invariant  $\Delta$  (finding results consistent with ref. 15 and 30) and refer to it in what follows. For inhomogeneous driving we initially let  $\Delta_i$  be smoothly varying as  $\Delta_i(y_i) = \bar{\Delta} + \Delta_0 \sin\left(\frac{2\pi y_i}{L_y}\right)$ , Fig. 2(a) [Inset].

The inputs to our model are thus  $\bar{\phi}$ ,  $\bar{\Delta}$ ,  $\Delta_0$  and  $L_y$ , while the

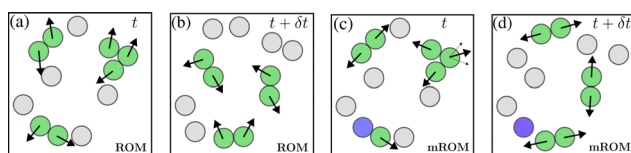


**Fig. 1** Schematic representations of the dynamical rules for the previously studied random organisation model (ROM)<sup>15</sup> ((a) and (b)) and the modified random organisation model (mROM) studied here ((c) and (d)). In both cases, isolated particles (grey) are inactive, while particles in contact with other particles (green) are active. In ROM, active particles are displaced by a random amount,  $\Delta$ , in a random direction, as indicated by black arrows. In contrast, in mROM, an active particle is displaced by a fixed  $\Delta$  in the direction of the resultant unit vector formed by all unit vectors connecting the particle to the centres of its neighbouring particles. The blue particle in mROM, which is relevant for Section 3.3, is assigned to  $\Delta = 0$  and remains pinned in its position.

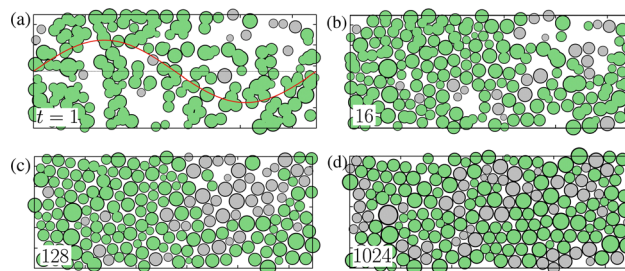


**Fig. 2** Time evolution of the system, starting from (a) a randomly generated configuration with many particle overlaps. The system continues to evolve through successive times (b)–(c) until a steady state is attained (d) for  $\bar{\phi} = 0.805$ ,  $\bar{\Delta} = 0.0515$ , and  $\Delta_0 = 0.03$ . The green and grey colours represent active and inactive particles, respectively. The red line schematically represents the spatial variation of  $\Delta(y)$ .

observables we compute are the spatial profiles of the area fraction

$\phi(y) = \frac{1}{L_x} \int_0^{L_x} \phi(x, y) dx$  and the active particle concentration  $C_A(y) = N_A(y)/N(y)$ , with  $N_A(y)$  and  $N(y)$  the number of active and total number of particles at position  $y$ . Coarse grained profiles are computed by binning particles in  $y$  before averaging the particle properties in each bin. Results are averaged across 50 realisations.

We define the order parameter  $\bar{C}_A = \frac{1}{L} \int_0^L C_A(y) dy$ , and  $\bar{C}_A^\infty$  as its steady state value. All the simulations presented here are carried out with periodic boundary conditions.

## 3. Results

### 3.1. Smoothly varying $\Delta(y)$

Using sinusoidal  $\Delta(y)$  we explore a range of  $\bar{\Delta}$  (letting  $\Delta_0 = 0.03$ ),  $\bar{\phi}$  and  $L_y$ , to investigate conditions that in principle span across the homogeneous absorbing state phase boundary. The typical time evolution of particles, starting from a randomly generated configuration with high particle overlap, is presented in Fig. 2. Model predictions are shown in Fig. 3. Inhomogeneous driving produces steady states with spatially varying  $\phi$ , with regions of higher  $\Delta(y)$  having lower  $\phi(y)$ , Fig. 3(a), in agreement with experiment<sup>31,32</sup> and simulations with more detailed physics.<sup>21,22,33</sup> The local active particle concentration  $C_A(y)$  varies in the opposite direction to  $\phi(y)$  at small  $t$ , before reaching steady states that are spatially uniform, Fig. 3(b). For  $(\bar{\phi}, \bar{\Delta})$  above the homogeneous phase boundary (top panels of (a) and (b)), the inhomogeneous system remains diffusive at long times with  $C_A(y) > 0$ , whereas below the homogeneous phase boundary  $C_A(y) = 0$  everywhere in the system. The system never produces mixed absorbing–diffusive steady states with  $C_A(y)$  only locally vanishing.

Each inhomogeneous simulation produces a set of parametric points corresponding to lines across the  $\Delta$ - $\phi$  phase diagram, bounded by  $\Delta = \bar{\Delta} \pm \Delta_0$ , Fig. 3(c). Initial states with uniform  $\phi(y)$  appear as vertical  $\Delta$ - $\phi$  lines, before evolving with time. Since the local activity at  $y$  is controlled by  $\phi(y)$  and  $\Delta(y)$ , particles in regions with higher  $\Delta$  have higher mobility and move to regions with lower  $\Delta$ , resulting in an increment of  $\phi$

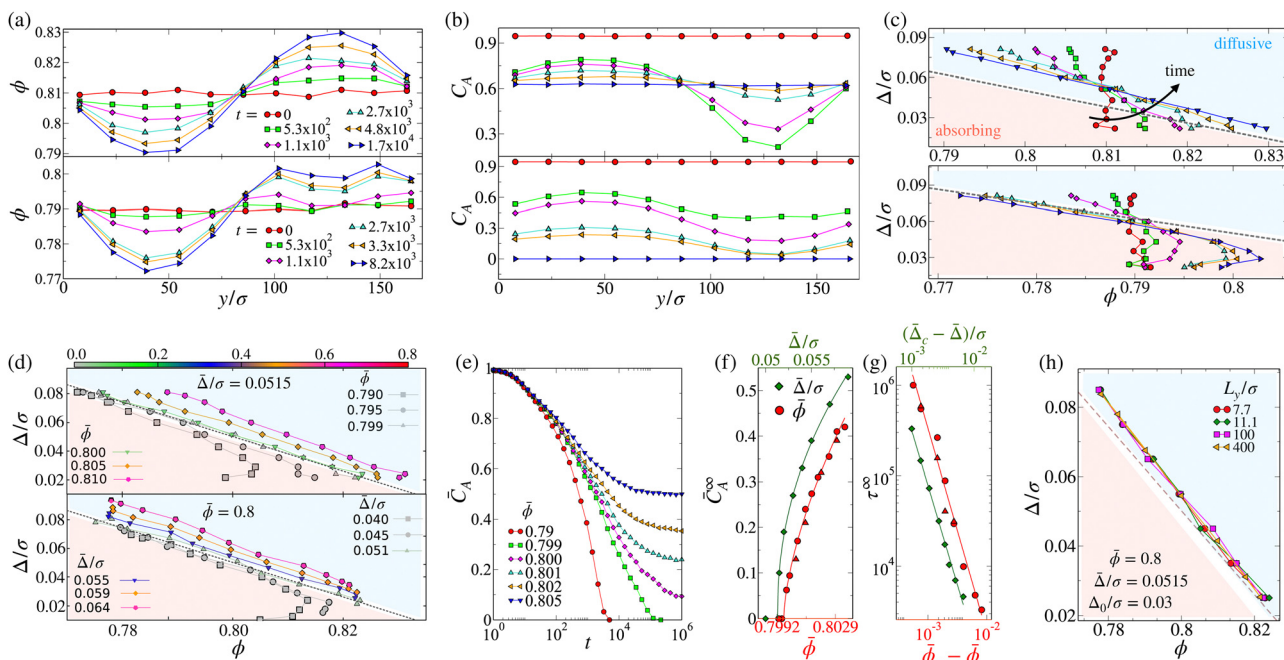


**Fig. 3** Absorbing-state transition in inhomogeneously driven particulate material, showing the time evolution of spatial variation of (a) area fraction  $\phi(y)$  and (b) active particle concentration  $C_A(y)$ , for systems that have steady states above (top,  $\bar{\phi} = 0.81$ ) and below (bottom,  $\bar{\phi} = 0.79$ ) the absorbing phase boundary, with  $\bar{\Delta}/\sigma = 0.0515$ ,  $\Delta_0/\sigma = 0.03$  and  $L_y/\sigma = 160$ . (c) The  $\Delta$ - $\phi$  phase space showing parametrically  $\phi(y)$  and  $\Delta(y)$  at progressing time. The dashed line is the homogeneous phase boundary separating absorbing (pink) and diffusive (blue) states (legend in (a) applies also to (b) and (c)); (d) Steady state  $\Delta$ - $\phi$  lines for  $\bar{\Delta} = 0.0515$  at a range of  $\bar{\phi}$  (top) and  $\bar{\phi} = 0.8$  at a range of  $\bar{\Delta}$  (bottom), with  $\Delta_0 = 0.03$ . The color bar represents the magnitude of  $C_A(y)$ ; (e) Time evolution of mean active concentration  $\bar{C}_A$  for various  $\bar{\phi}$  keeping  $\bar{\Delta}$ ,  $\Delta_0$  fixed; (f) Variation of  $\bar{C}_A^\infty$  with  $\bar{\phi}$  at fixed  $\bar{\Delta}$  (green) and  $\bar{\Delta}$  at fixed  $\bar{\phi}$  (red (circles:  $L_y/\sigma = 120$ ; triangles:  $L_y/\sigma = 11$ )); (g) Time  $\tau^\infty$  to reach absorbing state below the phase boundary, with  $\bar{\phi}$  (red) and  $\bar{\Delta}$  (green). Solid lines in (f) and (g) are fits to  $f(x) = f_0(x - x_c)^2$ ; (h) example steady state  $\Delta$ - $\phi$  lines (parameters in legend) showing independence of  $L_y$  in the diffusive regime.

and increase in activity in those regions. Thus, regions with initial local parameters below the absorbing phase boundary can increase in  $\phi(y)$  and thus become active. This process manifests as a counterclockwise rotation of  $\Delta$ - $\phi$ , Fig. 3(c) (top). For  $(\bar{\phi}, \bar{\Delta})$  above the homogeneous phase boundary, after this transient the system attains a diffuse steady state with  $\Delta(y)$  and  $\phi(y)$  balanced such that  $C_A(y)$  becomes spatially uniform. For  $(\bar{\phi}, \bar{\Delta})$  below the phase boundary, the large- $\Delta$  regions do not inject enough particles to the small- $\Delta$  regions to trigger activity, thus leaving those areas with the same conditions as at the beginning of the simulation and the resultant hook shape in Fig. 3(c) (bottom). Fig. 3(d) shows steady state  $\Delta$ - $\phi$  lines as functions of  $\bar{\phi}$  and  $\bar{\Delta}$ . The colorbar stands for the magnitude of  $C_A(y)$ , which decreases as  $(\bar{\phi}, \bar{\Delta})$  approaches the phase boundary from the diffusive phase and vanishes in the absorbing state. Interestingly, the location of the critical line where  $C_A(y)$  vanishes overlaps with the homogeneous phase boundary (dashed lines, Fig. 3(d)), so in principle a single inhomogeneous simulation can identify the entire homogeneous phase boundary. In Fig. 3(e) the variation of  $\bar{C}_A$  with time is shown for various  $\bar{\phi}$  at fixed  $\bar{\Delta}$ ,  $\Delta_0$ . As in the homogeneous case,  $\bar{C}_A$  vanishes at low  $\bar{\phi}$ , indicating that absorbing states exist, whereas above it saturates to non-zero steady states  $\bar{C}_A^\infty$  characterised by fitting the data to  $C_A(t) = c_0 e^{-(t/t_0)c_1} + \bar{C}_A^\infty$ , where  $c_0$ ,  $t_0$  and  $c_1$  are constants.

As  $\bar{C}_A^\infty$  serves as our order parameter, we investigate the details of the absorbing state transition by examining its dependence on the parameters. The measured values follow  $\bar{C}_A^\infty \sim (\bar{\phi} - \bar{\phi}_c)^{\beta_\phi}$  for fixed  $\bar{\Delta}$  and  $\bar{C}_A^\infty \sim (\bar{\Delta} - \bar{\Delta}_c)^{\beta_\Delta} \bar{\Delta}$  for fixed  $\bar{\phi}$ , Fig. 3(f), and we find  $\beta_\phi = 0.64$ , in agreement with ref. 16 and 28  $\bar{\phi}_c = 0.7996$ , and  $\beta_\Delta = 0.45$ , close to the values reported by ref. 5, with  $\bar{\Delta}_c = 0.0513$ . Additionally, as the system approaches the critical line from the absorbing phase, the time required to reach steady state diverges as  $\tau^\infty \sim (\bar{\phi} - \bar{\phi}_c)^{\nu_\phi}$  for fixed  $\bar{\Delta}$  and  $\tau^\infty \sim (\bar{\Delta} - \bar{\Delta}_c)^{\nu_\Delta}$  for fixed  $\bar{\phi}$ , Fig. 3(g). We find  $\nu_\phi = 1.37$  with  $\bar{\phi}_c = 0.7994$ , and  $\nu_\Delta = 1.33$  with  $\bar{\Delta}_c = 0.0513$ , in close agreement with previous studies.<sup>5,16,28</sup> Thus the position and nature of the phase boundary obtained under inhomogeneous conditions matches the homogeneous case. We verified that this holds for  $L_y/\sigma = 7.7$ –400, Fig. 3(f)–(h). We do not run simulations for driving wavelengths smaller than 7.7, since driving with a wavelength comparable to the particle size is not effectively smooth.

### 3.2 Continuum model

Given that the phase boundary is governed by local conditions only, we introduce a continuum model (Manna class<sup>34,35</sup> without noise<sup>36</sup>) modified for inhomogeneous driving by introducing convection in the system. Herein  $\phi_A(y, t)$  and  $\phi_I(y, t)$  are the area fraction of active and inactive particles, related through

$\phi(y, t) = \phi_A(y, t) + \phi_I(y, t)$ ,  $\dot{\phi} = \dot{\phi}_A + \dot{\phi}_I$ , and with  $C_A = \phi_A/\phi$ . The dynamics are given by

$$\dot{\phi}_A = \frac{\partial}{\partial y} \left( \mathcal{D} \frac{\partial \phi_A}{\partial y} \right) + \frac{\partial}{\partial y} (\mathbf{v} \phi_A) + \alpha \phi_A (\phi - \phi_A) - \gamma \phi_A (1 - \phi), \quad (1)$$

$$\dot{\phi}_I = -\alpha \phi_A (\phi - \phi_A) + \gamma \phi_A (1 - \phi), \quad (2)$$

where  $\alpha$  and  $\gamma$  are positive coefficients.  $\alpha$  represents activation of particles by interaction with active neighbours;  $\gamma$  represents isolated death (we omit caging<sup>37</sup>). The convection term in eqn (1) arises due to spatially varying driving, where  $\mathbf{v}$  is given by  $\delta \Delta / \tau$ , with  $\delta \Delta = \Delta(y + \delta y) - \Delta(y)$ , and  $\tau$  is the timescale, taken as unity. The diffusion coefficient is given by  $\mathcal{D}(y) \sim \Delta^2(y)/\tau$ . The phase boundary can be estimated from the condition  $\phi_A = 0$ ,  $\nabla \phi_A = 0$  and  $\dot{\phi}_A = 0$ . The coefficient  $\alpha$  is directly related to  $\Delta$ , and for simplicity we choose  $\alpha \sim \Delta$ . Thus, the critical mean kick size  $\bar{\Delta}_c$  representing the phase boundary at a fixed  $\bar{\phi}$  is  $\bar{\Delta}_c = \gamma/\bar{\phi} - \gamma$ .

We solve these coupled equations numerically, with  $\Delta(y) = \bar{\Delta} + \Delta_0 \sin\left(\frac{2\pi y}{L_y}\right)$  and initial conditions  $\phi(y) = \bar{\phi} = 0.83$ ,  $\phi_A(y) = \phi_A^0 = 0.65$  using  $\bar{\Delta} = 0.35$ ,  $\Delta_0 = 0.05$ . Shown in Fig. 4(a)–(c) are transients of  $\phi(y)$  and  $C_A(y)$  in the diffusive regime, showing qualitative agreement with Fig. 3(a)–(c) (top). In Fig. 4(d) are steady state  $\Delta$ – $\phi$  lines spanning the absorbing phase boundary, qualitatively matching the random organization model predictions in Fig. 3(d). In the absorbing state (gray lines) the hook shape in  $\Delta$ – $\phi$  appears as in the simulation, though with a sharper curve and a vertical profile at lower  $\Delta$  where the dynamics cease quickly. The evolution of  $\bar{C}_A$  with time is shown in Fig. 4(e), approaching 0 and finite values respectively below and above the phase boundary with the time scale  $\tau$  diverging at the transition. We find  $\bar{C}_A^\infty \sim (\bar{\phi} - \bar{\phi}_c)\beta_c$ , with  $\beta_c = 1$  agreeing with previously reported results<sup>29,37</sup> for homogeneous driving.

### 3.3. Discontinuous $\Delta(x, y)$

Next, we scrutinize the random organization model under discontinuously varying  $\Delta(x, y)$ , where  $(x, y)$  represents the coordinates of the centre of a cell. To do so we divide the system into cells of area  $L_c^2$ , each having  $\Delta = \bar{\Delta} + \Delta_r$ , with  $\Delta_r$  a random number chosen uniformly in the range  $\pm \Delta_0$ , ensuring  $\sum_{i=1}^{N_c} \Delta_r = 0$ , where  $N_c$  is the number of cells.  $\Delta_r$  assigned to every cell is different for different realizations. Unlike smoothly varying  $\Delta$ , in this case,  $\Delta$  can vary in both directions. We verified our results for setups where  $\Delta$  varies in either the  $x$ - or the  $y$ -direction and found no qualitative difference. We verified that the cell area is the key control parameter in what follows; we show results for square cells though other aspect ratios produce equivalent results provided the shorter length scale exceeds the particle size. A schematic diagram of the system is presented in Fig. 5(e), inset, showing how the system is divided into many cells, with the colour of each cell representing the magnitude of  $\Delta$  for that cell. Model predictions are

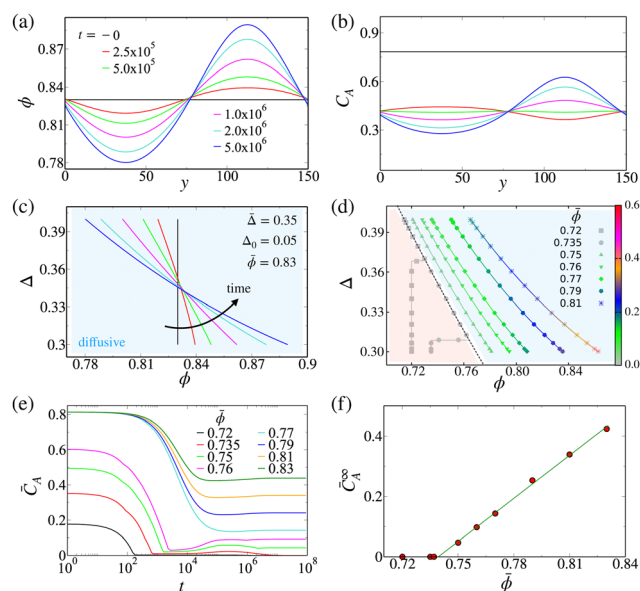
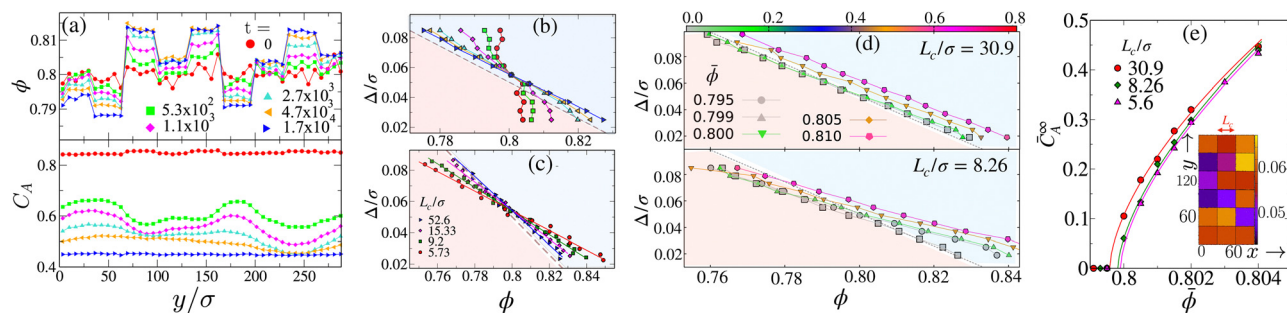


Fig. 4 Predictions of continuum model. Shown are the time evolution of (a)  $\phi(y)$ , (b)  $C_A(y)$  and (c) the  $\Delta$ – $\phi$  line, from initialization up to a steady state in the diffusive regime (parameters in legend of (c)). The color scale in (a) applies also to (b) and (c); (d) steady state  $\Delta$ – $\phi$  lines for various  $\bar{\phi}$  at fixed profiles of  $\Delta(y)$ ; color bar shows the magnitude of  $C_A(y)$ . (e) Time evolution of  $\bar{C}_A$  for a range of  $\bar{\phi}$  spanning the absorbing phase boundary; (f) variation of  $\bar{C}_A^\infty(y)$  with  $\bar{\phi}$  keeping the  $\Delta(y)$  profile fixed, with a solid line as in Fig. 3(f).

shown in Fig. 5. The transients observed for exemplar model parameters match qualitatively those from the smoothly varying model, Fig. 5(a). Although the local volume fraction and concentration of active particles vary spatially in both the  $x$  and  $y$  directions, the figure shows the variation in the  $y$  direction by averaging over the particles within each cell that share the same  $x$  coordinate. In the steady state (blue points),  $\phi(y)$  is uniform within each cell but changes sharply at the boundaries between cells due to the variation in  $\Delta$  (Fig. 5(a), top panel). As in the smoothly varying case, active particles are distributed uniformly in the diffusive regime, (Fig. 5(a), bottom panel). However, steady state  $\Delta$ – $\phi$  data deviate significantly from the homogeneous absorbing state phase boundary, Fig. 5(b). For small  $L_c$ , states that would be deep within the absorbing state remain active. This indicates that under discontinuously varying driving the absence or presence of an absorbing state cannot be determined using local knowledge of  $\phi(y)$  and  $\Delta(y)$ : the size of the containing cell matters. Presumably particles near cell edges experience dynamics not described by eqn (1) and (2) due to proximal discontinuities in  $\Delta$ . Indeed, as  $L_c$  increases (and fewer particles are near edges), the data tend towards a diffusive line parallel to the homogeneous phase boundary as would be expected for locally governed dynamics. In Fig. 5(c) steady state  $\Delta$ – $\phi$  lines are shown for  $\bar{\Delta} = 0.0515$ ,  $\Delta_0 = 0.03$  and a set of  $\bar{\phi}$  crossing the homogeneous phase boundary (grey dotted line), for  $L_c/\sigma = 30.9$  and  $L_c/\sigma = 8.26$ . The overall trend is similar to smoothly varying  $\Delta(y)$ , but importantly the position of the boundary under randomly varying  $\Delta$  does not match the homogeneous case, especially at small  $L_c$ . In fact, even at the largest  $L_c$  investigated here we find a discrepancy



**Fig. 5** Model predictions with discontinuous  $\Delta(x, y)$ . Shown are panel (a) top, panel (a) bottom and panel (b) time evolution of the  $\phi(y)$ ,  $C_A(y)$  and  $\Delta-\phi$  for  $\bar{\phi} = 0.80$ , with  $\bar{\Delta} = 0.056$ ,  $\Delta_0 = 0.03$  and  $L_c/\sigma = 33.1$ , showing similar behaviour to the smoothly varying case. The sudden jumps in  $\phi(y)$  are due to the discontinuous nature of  $\Delta(x, y)$ . (c) Steady state  $\Delta-\phi$  lines for  $\bar{\phi} = 0.80$ ,  $\bar{\Delta} = 0.054$  and  $\Delta_0 = 0.03$ , as a function of cell size  $L_c$ . The dashed line shows homogeneous absorbing state phase boundary. (d) Steady state  $\Delta-\phi$  lines for  $\bar{\Delta} = 0.0515$ ,  $\Delta_0 = 0.03$  at different  $\bar{\phi}$  values for  $L_c = 30.9$  (top) and  $L_c = 8.26$  (bottom). Grey dotted lines are the homogeneous absorbing phase boundary and the color bar represents  $C_A(y)$ : (e) variation of  $\bar{C}_A^\infty$  with  $\bar{\phi}$ , keeping  $\bar{\Delta} = 0.0515$ , showing the changing position of the boundary with  $L_c$ . Solid lines follow the form in Fig. 3(f). Inset: Schematic representation of the system with random variation of  $\Delta(x, y)$ . Each grid has the same value of  $\Delta$ , with the colour representing its magnitude.

between the inhomogeneous and homogeneous phase boundaries, suggesting, as mentioned above, that the discontinuous variation in  $\Delta$  occurring at the cell edges qualitatively affects the material. Fig. 5(d) shows the variation of  $\bar{C}_A^\infty$  with  $\bar{\phi}$  at fixed  $\bar{\Delta}$  for a range of  $L_c$ . The exponents match those in Fig. 3(f), but crucially there is dependence of the critical point  $\bar{\phi}_c$  on  $L_c$ .

We finally test the model for a fundamentally different type of inhomogeneity in which a small subset of particles is permanently inactive. To do so we modify the above model by enforcing  $\Delta = 0$  for a small fraction  $C_p$  of particles, chosen randomly. The remaining particles are assigned a fixed  $\Delta$ , so that the mean kick size is now given by  $\bar{\Delta} = (1 - C_p)\Delta$ . Particles with  $\Delta = 0$  remain frozen in their initial positions, equivalent to a pinning effect used widely in fundamental studies of various systems.<sup>38–40</sup> See blue particle in Fig. 2(c). From one point of view, the pinned particles can be considered as special types of impurities (quenched disorder) that break the translational invariance of the system as well as introduce a new length scale controlled by the mean inter-pinned particle distance. Since the criticality associated with absorbing state transitions is governed by a diverging length scale, it would be interesting to

observe how the introduction of a length scale in the system affects the nature of the criticality. Moreover, particle pinning has recently been realized with the help of optical trapping in colloidal systems,<sup>41</sup> which provides an excellent setup for verifying the observations from our simulations. From another point of view, these particles can be considered obstacles through which the flow is maintained. A similar setup was recently used to study the reversible (absorbing)–irreversible (diffusive) transition for repulsive disks.<sup>42,43</sup>

We run these dynamics for a range of  $C_p$  and  $\bar{\phi}$ , with  $\Delta = 0.0515$ . Shown in Fig. 6(a) is the resultant variation of the steady state  $\bar{C}_A^\infty$ . The points are simulation data, and solid lines are fits to  $\bar{C}_A^\infty \sim (\phi - \phi_c)^\beta$ . The critical area fraction  $\bar{\phi}_c$  and exponent  $\beta$  both decrease with increasing  $C_p$ , Fig. 6(b) and (c), suggesting a change in the nature of criticality due to particle pinning,<sup>44</sup> which might arise due to potential shortening the range of interactions in the system.<sup>20,45,46</sup> The solid line in (b) represents a fit using the function  $\beta = ae^{-bx^c} + \beta_0$ , indicating that  $\beta$  approaches an asymptotic value of  $\beta_0 = 0.46$ . It is noteworthy that systems with  $C_p \geq 0.1$  exhibit different behaviour as the pinned particles percolate the system, effectively causing it to

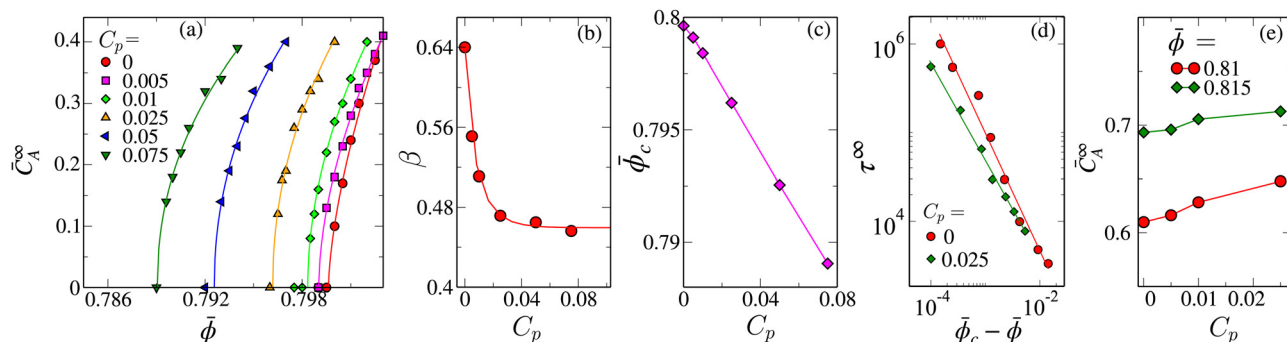


**Fig. 6** Absorbing state transition with permanently inactive particle fraction  $C_p$ . (a) Steady state mean active particle concentration  $\bar{C}_A^\infty$  as a function of  $\bar{\phi}$  for varying  $C_p$  with  $\Delta = 0.0515$ ; variation with  $C_p$  of (b) the critical exponent  $\beta$  and (c) the critical area fraction  $\bar{\phi}_c$ . The solid line in panel (b) is a fit using the function  $\beta = ae^{-bx^c} + \beta_0$  suggesting that  $\beta$  approaches an asymptotic value  $\beta_0 = 0.46$ . (d) Time  $\tau^\infty$  to reach absorbing state below the phase boundary with associated critical exponent  $\nu = 1.37$  and  $1.1$  for  $C_p = 0$  and  $0.025$ , respectively. In (e),  $\bar{C}_A^\infty$  versus  $C_p$  is plotted at two high volume fractions to illustrate the absence of any crossover in  $\bar{C}_A^\infty$  for systems with  $C_p = 0$  and  $C_p > 0$ , as suggested by the extrapolated fit in (a).

behave as a porous medium. At high  $C_p$ , active particles tend to form clusters that do not diffuse within the available simulation timescale. We also observe a change in the critical exponent  $\nu$  associated with the diverging time scale required to reach an absorbing state,  $\tau^\infty \sim (\bar{\phi}_c - \bar{\phi})^\nu$ . The exponent  $\nu$  decreases from 1.37 for  $C_p = 0$  to 1.1 for  $C_p = 0.025$ , providing further evidence of a departure from the CDP universality class due to particle pinning. It is important to clarify that although the extrapolation of solid fits in panel (a) suggests that at high  $\bar{\phi}$ , systems with higher  $C_p$  might have lower  $\bar{C}_A$ , such a crossover does not occur as shown in panel (d). This discrepancy arises because the functional form  $\bar{C}_A^\infty \sim (\phi - \phi_c)^\beta$  is valid only close to the critical point and tends to overestimate  $\bar{C}_A$  at large  $\bar{\phi}$ .

## 4. Conclusions

We study the absorbing state transition in particulate systems under inhomogeneous driving using a modified random organisation model, which produces spatial variation in  $\phi$ , resulting in distinct points in the  $\Delta$ - $\phi$  phase diagram. This behavior is replicated by a continuum description incorporating a convective term. The critical line separating absorbing from diffusive states is unchanged for smoothly varying driving, while for discontinuously varying driving, the position of the absorbing phase boundary can deviate, suggesting potential manipulation by altering the driving heterogeneity. Our findings indicate that, although homogeneous and inhomogeneous rheology of the particulate system differ qualitatively, in the case of the absorbing state transition, predictions from spatially homogeneous conditions apply only to inhomogeneous systems with smoothly varying driving, highlighting the need for further study of absorbing states under discontinuous driving.

In the presence of randomly pinned particles, the smooth variation of the critical exponent  $\beta$  towards an asymptotic value suggests a crossover from the CDP universality class to a new universality class. Such a crossover has been observed in other systems with quenched disorder.<sup>47,48</sup> However, fully understanding the true nature of this crossover requires systematic analysis across different system sizes. Furthermore, it remains unclear whether configurations at the critical point exhibit hyperuniformity in the presence of quenched disorder. Addressing these questions will require large-scale simulations, which will be explored in future work. In addition to this, the study is limited to the regime below jamming. However, an absorbing state transition is also observed in the athermal cyclic deformation of glassy systems,<sup>2,49–54</sup> where the transition is discontinuous. Investigating such transitions above the jamming volume fraction, under heterogeneous conditions using a modified model,<sup>18</sup> presents an intriguing direction for future work.

From a practical perspective, absorbing state transitions, and the associated process of random organisation, are relevant to the burgeoning area of active viscosity control in dense suspension rheology.<sup>55</sup> In a recent series of articles it has been demonstrated that acoustic modulation provides fine control over suspension viscosity,<sup>56,57</sup> and similar approaches have

been demonstrated in practical applications.<sup>58,59</sup> Here it is likely that the vibrations are attenuated with growing distance from the source, so that random organisation under spatially inhomogeneous driving, as we study in this article, is the relevant mechanism driving the viscosity reduction. Moreover, while we focus on particulate systems, our findings may also prove beneficial for understanding absorbing states in other systems characterized by spatial inhomogeneities in the control parameters.

## Data availability

The main text contains all the data and the theoretical basis to construct the data.

## Conflicts of interest

There are no conflicts to declare.

## Acknowledgements

B. P. B. acknowledges support from the Leverhulme Trust under Research Project Grant RPG-2022-095; C. N. acknowledges support from the Royal Academy of Engineering under the Research Fellowship scheme.

## Notes and references

- H. Hinrichsen, *Adv. Phys.*, 2000, **49**, 815–958.
- H. Bhaumik, G. Foffi and S. Sastry, *Proc. Natl. Acad. Sci. U. S. A.*, 2021, **118**, e2100227118.
- D. Bonn, M. M. Denn, L. Berthier, T. Divoux and S. Manneville, *Rev. Mod. Phys.*, 2017, **89**, 035005.
- B. P. Bhowmik, H. G. E. Hentchel and I. Procaccia, *Europhys. Lett.*, 2022, **137**, 46002.
- L. Corté, P. M. Chaikin, J. P. Gollub and D. J. Pine, *Nat. Phys.*, 2008, **4**, 420–424.
- Y. Huang and M. Yu, *Nat. Hazards*, 2013, **65**, 2375–2384.
- A. Janda, D. Maza, A. Garcimartín, E. Kolb, J. Lanuza and E. Clément, *Europhys. Lett.*, 2009, **87**, 24002.
- D. J. Pine, J. P. Gollub, J. F. Brady and A. M. Leshansky, *Nature*, 2005, **438**, 997–1000.
- L. Corté, S. J. Gerbode, W. Man and D. J. Pine, *Phys. Rev. Lett.*, 2009, **103**, 248301.
- K. A. Takeuchi, M. Kuroda, H. Chaté and M. Sano, *Phys. Rev. Lett.*, 2007, **99**, 234503.
- K. Hima Nagamanasa, S. Gokhale, A. K. Sood and R. Ganapathy, *Phys. Rev. E: Stat., Nonlinear, Soft Matter Phys.*, 2014, **89**, 062308.
- D. Fiocco, G. Foffi and S. Sastry, *Phys. Rev. E: Stat., Nonlinear, Soft Matter Phys.*, 2013, **88**, 020301.
- J. Wang, J. M. Schwarz and J. D. Paulsen, *Nat. Commun.*, 2018, **9**, 2836.
- C. F. Schreck, R. S. Hoy, M. D. Shattuck and C. S. O'Hern, *Phys. Rev. E: Stat., Nonlinear, Soft Matter Phys.*, 2013, **88**, 052205.

- 15 E. Tjhung and L. Berthier, *Phys. Rev. Lett.*, 2015, **114**, 148301.
- 16 L. Galliano, M. E. Cates and L. Berthier, *Phys. Rev. Lett.*, 2023, **131**, 047101.
- 17 D. Hexner and D. Levine, *Phys. Rev. Lett.*, 2015, **114**, 110602.
- 18 C. Ness and M. E. Cates, *Phys. Rev. Lett.*, 2020, **124**, 088004.
- 19 A. Ghosh, J. Radhakrishnan, P. M. Chaikin, D. Levine and S. Ghosh, *Phys. Rev. Lett.*, 2022, **129**, 188002.
- 20 R. Mari, E. Bertin and C. Nardini, *Phys. Rev. E*, 2022, **105**, L032602.
- 21 K. Saitoh and B. P. Tighe, *Phys. Rev. Lett.*, 2019, **122**, 188001.
- 22 B. P. Bhowmik and C. Ness, *Phys. Rev. Lett.*, 2024, **132**, 118203.
- 23 J. Goyon, A. Colin, G. Ovarlez, A. Ajdari and L. Bocquet, *Nature*, 2008, **454**, 84–87.
- 24 K. Kamrin and G. Koval, *Phys. Rev. Lett.*, 2012, **108**, 178301.
- 25 P. Chaudhuri, V. Mansard, A. Colin and L. Bocquet, *Phys. Rev. Lett.*, 2012, **109**, 036001.
- 26 P. Chaudhuri and J. Horbach, *Phys. Rev. E: Stat., Nonlinear, Soft Matter Phys.*, 2014, **90**, 040301.
- 27 L. Milz and M. Schmiedeberg, *Phys. Rev. E: Stat., Nonlinear, Soft Matter Phys.*, 2013, **88**, 062308.
- 28 S. Lübeck, *Int. J. Mod. Phys. B*, 2004, **18**, 3977–4118.
- 29 G. I. Menon and S. Ramaswamy, *Phys. Rev. E: Stat., Nonlinear, Soft Matter Phys.*, 2009, **79**, 061108.
- 30 P. Pham, J. E. Butler and B. Metzger, *Phys. Rev. Fluids*, 2016, **1**, 022201.
- 31 S. Oh, Y.-q. Song, D. I. Garagash, B. Lecampion and J. Desroches, *Phys. Rev. Lett.*, 2015, **114**, 088301.
- 32 R. E. Hampton, A. A. Mammoli, A. L. Graham, N. Tetlow and S. A. Altobelli, *J. Rheol.*, 1997, **41**, 621–640.
- 33 J. J. J. Gillissen and C. Ness, *Phys. Rev. Lett.*, 2020, **125**, 184503.
- 34 A. Vespignani and S. Zapperi, *Phys. Rev. Lett.*, 1997, **78**, 4793–4796.
- 35 A. Vespignani, R. Dickman, M. A. Muñoz and S. Zapperi, *Phys. Rev. Lett.*, 1998, **81**, 5676–5679.
- 36 A. Hipke, S. Lübeck and H. Hinrichsen, *J. Stat. Mech.: Theory Exp.*, 2009, **2009**, P07021.
- 37 S.-L.-Y. Xu and J. M. Schwarz, *Phys. Rev. E: Stat., Nonlinear, Soft Matter Phys.*, 2013, **88**, 052130.
- 38 C. Cammarota and G. Biroli, *Proc. Natl. Acad. Sci. U. S. A.*, 2012, **109**, 8850–8855.
- 39 R. Das, B. P. Bhowmik, A. B. Puthirath, T. N. Narayanan and S. Karmakar, *Proc. Natl. Acad. Sci. U. S. A.*, 2023, **2**, pgad277.
- 40 B. P. Bhowmik, P. Chaudhuri and S. Karmakar, *Phys. Rev. Lett.*, 2019, **123**, 185501.
- 41 S. Gokhale, K. Hima Nagamanasa, R. Ganapathy and A. K. Sood, *Nat. Commun.*, 2014, **5**, 4685.
- 42 C. Reichhardt and C. J. O. Reichhardt, *J. Chem. Phys.*, 2022, **156**, 124901.
- 43 D. Minogue, M. R. Eskildsen, C. Reichhardt and C. J. O. Reichhardt, *Phys. Rev. E*, 2024, **109**, 044905.
- 44 B. P. Bhowmik, S. Karmakar, I. Procaccia and C. Rainone, *Phys. Rev. E*, 2019, **100**, 052110.
- 45 L. Angelani, M. Paoluzzi, G. Parisi and G. Ruocco, *Proc. Natl. Acad. Sci. U. S. A.*, 2018, **115**, 8700–8704.
- 46 T. Jocteur, S. Figueiredo, K. Martens, E. Bertin and R. Mari, *Phys. Rev. Lett.*, 2024, **132**, 268203.
- 47 R. C. Vásquez, V. R. Paredes, A. Hasmy and R. Jullien, *Phys. Rev. Lett.*, 2003, **90**, 170602.
- 48 J. Yoon, D. Sergatskov, J. Ma, N. Mulders and M. H. W. Chan, *Phys. Rev. Lett.*, 1998, **80**, 1461–1464.
- 49 I. Regev, T. Lookman and C. Reichhardt, *Phys. Rev. E: Stat., Nonlinear, Soft Matter Phys.*, 2013, **88**, 062401.
- 50 C. Reichhardt, I. Regev, K. Dahmen, S. Okuma and C. J. O. Reichhardt, *Phys. Rev. Res.*, 2023, **5**, 021001.
- 51 N. C. Keim and P. E. Arratia, *Phys. Rev. Lett.*, 2014, **112**, 028302.
- 52 T. Kawasaki and L. Berthier, *Phys. Rev. E*, 2016, **94**, 022615.
- 53 E. Tjhung and L. Berthier, *Phys. Rev. E*, 2017, **96**, 050601.
- 54 W.-T. Yeh, M. Ozawa, K. Miyazaki, T. Kawasaki and L. Berthier, *Phys. Rev. Lett.*, 2020, **124**, 225502.
- 55 C. Ness, R. Mari and M. E. Cates, *Sci. Adv.*, 2018, **4**, eaar3296.
- 56 P. Sehgal, M. Ramaswamy, I. Cohen and B. J. Kirby, *Phys. Rev. Lett.*, 2019, **123**, 128001.
- 57 C. Garat, S. Kiesgen de Richter, P. Lidon, A. Colin and G. Ovarlez, *J. Rheol.*, 2022, **66**, 237–256.
- 58 G. Hong, J. Gao, Q. Zheng, A. Yu and S. Liu, *Int. J. Mech. Sci.*, 2025, 110128.
- 59 J. R. Lawrence, H. R. Lipic, T. D. Manship and S. F. Son, *npj Adv. Manuf.*, 2024, **1**, 5.